Probing the metallic energy spectrum beyond the Thouless energy scale using singular value decomposition

Richard Berkovits
Department of Physics, Jack and Pearl Resnick Institute, Bar-Ilan University, Ramat-Gan 52900, Israel

(Received 20 July 2021; accepted 12 August 2021; published 23 August 2021)

Disordered quantum systems feature an energy scale known as the Thouless energy. For energy ranges below this scale, the properties of the energy spectrum can be described by random matrix theory. Above this scale a different behavior sets in. For a metallic system it was shown long ago by Altshuler and Shklovskii [Sov. Phys. JETP **64**, 127 (1986)] that the number variance should increase as a power law with power dependent on only the dimensionality of the system. Although tantalizing hints at this behavior were seen in previous numerical studies, it is quite difficult to verify this prediction using the standard local unfolding methods. Here we use a different unfolding method, i.e., singular value decomposition, and establish a connection between the power law behavior of the scree plot (the singular values ranked by their amplitude) and the power law behavior of the number variance. Thus, we are able to numerically verify Altshuler and Shklovskii's prediction for disordered three-, four-, and five-dimensional single-electron Anderson models on square lattices in the metallic regime. The same method could be applied to systems such as the Sachdev-Ye-Kitaev model and various interacting many-body models for which the many-body localization occurs. It was recently reported that such systems exhibit a Thouless energy, and analyzing the spectrum's behavior on larger scales is of much current interest.

DOI: 10.1103/PhysRevB.104.054207

I. INTRODUCTION

Weakly disordered quantum systems are known to exhibit a universal behavior of their energy spectrum which depends on only the symmetry of the system [1]. The statistical properties of the energy spectrum do not depend on the details of the system and are described by a random matrix model with the same symmetry. This behavior is extremely useful in identifying and understanding various properties of metallic systems [2–6].

As pointed out by Altshuler and Shklovskii [7], this universal behavior holds only for energy scales which are below the Thouless energy E_T. The Thouless energy corresponds to $E_T = \hbar/t_T$, where the Thouless time $t_T = L^2/D$ (L is the linear dimension of the sample, and D is the diffusion constant) depicts the time it takes for a diffusing particle to sample the whole system. For shorter times the motion is not yet diffusive and therefore dependent on details of the local system. Thus, above this energy scale, the behavior of statistical properties of the spectrum will diverge from the random matrix predictions. The canonical measure used to probe this deviation is the number variance [1], defined as the variance in the number of energy levels within an energy window for an unfolded energy spectrum. Defining a window of size E, one can count the number of levels within this window for a given realization of disorder and obtain the average number of levels $\langle n(E)\rangle$ and the variance $\langle \delta^2 n(E)\rangle = \langle [n(E) - \langle n(E)\rangle]^2\rangle$, where $\langle \cdots \rangle$ denotes an average over an ensemble of different realizations of disorder. For the Wigner-Dyson random matrix ensemble [Gaussian orthogonal ensemble (GOE)] $\langle \delta^2 n(E)\rangle = 0.44 + (2/\pi^2)\ln[\langle n(E)\rangle]$, while for the localized regime $\langle \delta^2 n(E)\rangle = \langle n(E)\rangle$. Metallic systems correspond to the Wigner-Dyson random matrix predictions up to an energy window of size E_T, and Altshuler and Shklovskii [7] predicted that for $E > E_T$ the number variance will follow $\langle \delta^2 n(E)\rangle \propto \langle n(E)\rangle^{d/2}$, where d is the dimensionality.

The deviation of the number variance from the random matrix logarithmic behavior to a stronger than linear behavior at large energies has been observed in metallic systems [8,9]. Recently, it has gained much interest beyond traditional single-particle disordered systems. Stronger than linear deviations of the number variance beyond a certain energy scale have been seen in the context of the Sachdev-Ye-Kitaev (SYK) model [10,11], many-body localization systems [12–15], and the generalized Rosenzweig-Porter random matrix model [16,17]. In all these cases it was argued that the energy for which the number variance becomes stronger than linear corresponds to the inverse of the timescale for which the motion can no longer sample the entire phase space.

Although the prediction for the behavior of the number variance on scales larger than the Thouless energy is straightforward, it is not easy to corroborate even for simple single-particle systems such as the Anderson model with any degree of certainty. We shall see that the main problem is the local unfolding procedure, as has been noted by previous studies [15,18].

Here we intend to address this challenge of verifying Altshuler and Shklovskii prediction [7]. We shall illustrate in detail that a straightforward study of the number variance using local unfolding is fraught with ambiguities. Therefore, it is clear that a different tack is needed. Here we will suggest a couple of different measures which are based on the singular value decomposition (SVD) method. This method has been used to classify whether a system follows Wigner or Poisson

statistics [19–21] and, recently, to identify the nonergodic extended signature in the Rosenzweig-Porter model [22]. As we shall demonstrate, using the SVD method to replace the short-range unfolding provides a clearer way to study the behavior of the energy spectrum beyond the Thouless energy.

This paper is organized as follows. In Sec. II we define the single-particle Anderson model on a square lattice for different dimensionalities. Section III presents the numerical results for the number variance using local unfolding and discusses the challenges it presents. Section IV shows the use of the SVD to tease out the behavior of the large energy scales. In Sec. IV A we give an overview of the SVD method. In Sec. IV B we use the SVD to perform a global unfolding by filtering out the low modes of the singular values which correspond to the global features of the energy spectrum, thus retaining only the fluctuations. Establishing analytically a connection between the power spectrum of these fluctuations and the number variance enables us to glean the long-range behavior of the energy spectrum. Since there is a connection between the power spectrum and the scree plot of the singular value modes (the singular values ranked by their amplitude), as established in Sec. IV B, the scree plot may be used to read off the long-range spectrum properties. It is used in Sec. IV C in order to verify the dependence of the number variance on dimensionality. Issues related to the number of eigenvalues taken into account and the number of realizations of disorder considered are also discussed. In Sec. V we discuss the possibility of applying the SVD to additional interesting systems such as the Sachdev-Ye-Kitaev model and disordered interacting many-body models known to exhibit many-body localization.

II. MODEL

We consider a simple one-particle Anderson model on a d-dimensional square lattice with sites at $\vec{r} = j_x\hat{x} + j_y\hat{y} + \cdots$, where $j_i = 1, 2, \ldots, L_i$ and L_i is the length in the $\hat{i}$ direction. Each site has an on-site energy $\epsilon_{\vec{r}}$ chosen randomly from a box distribution in the range $-W/2 \cdots W/2$. Nearest-neighbor hopping between the sites is considered, with a hopping matrix element set to 1. Thus, the Hamiltonian is written as

$$H = \sum_{\vec{r}} \epsilon_{\vec{r}} c^{\dagger}_{\vec{r}} c_{\vec{r}} + \sum_{\vec{r}} \sum_{\hat{a}} c^{\dagger}_{\vec{r}+\hat{a}} c_{\vec{r}}, \tag{1}$$

where $c^{\dagger}_{\vec{r}}$ is the creation operator at site $\vec{r}$ and $\hat{a} = \pm\hat{x}, \pm\hat{y}, \ldots$ are unit vectors to the nearest-neighbor sites.

This model is known to exhibit a metal-insulator transition at a critical disorder $W_C = 16.5$ for the three-dimensional (3D_ case, $W_C = 34.5$ for the four-dimensional (4D) case, and $W_C = 57.5$ for the five-dimensional (5D) case [23]. In order to study the long-range spectra behavior deep in the metallic regime, we concentrate on values of disorder much lower than the critical disorder, i.e., $W = 5$ and $W = 10$. Using exact diagonalization, we calculate the eigenvalues for the $L^d \times L^d$ matrices, where we consider hypercubes of size $L = L_x = L_y \cdots$ and hard-wall boundary conditions. For the 3D case we consider sizes $L = 20, 24, 28$, corresponding to $L^3 = 8000, 13\,824, 21\,952$, while in the 4D case we evaluate sizes $L = 9, 10, 11, 12, 13$, resulting in $L^4 = 6561, 10\,000, 14\,641, 20\,736, 29\,561$, and for the 5D case we consider $L = 6, 7, 8$, which amounts to $L^5 = 7776, 16\,807, 32\,768$. Unless noted differently, in all cases the spectra were calculated for 3000 different realizations.

III. NUMBER VARIANCE

To begin, we shall investigate the behavior of number variance at large energies as a function of the dimensionality and system size. Using the L^d eigenvalues ϵ_i obtained for each realization, the spectrum is locally unfolded. The following local unfolding was applied: each eigenvalue obtains the value $\varepsilon_i = \varepsilon_{i-1} + 2p(\epsilon_i - \epsilon_{i-1})/\langle\epsilon_{i+p} - \epsilon_{i-p}\rangle$, where $\langle\cdots\rangle$ is an average over realizations, and we have checked that the results are not very sensitive to the value of p (for all results presented here $p = 6$ was chosen). The number variance is also averaged over 41 positions of the center of the energy window $E(k)$, equally spaced around the band center, where the farthest point is no more than $1/15$ of the bandwidth from the center. For each $E(k)$, the number of states in a window of width E centered at $E(k)$, $n_k(E)$, is evaluated; then the averages $\langle n(E)\rangle$ and $\langle n^2(E)\rangle$ are taken over all positions of the center k and all realizations.

One expects that for $E < E_T$, the number variance will follow the Wigner Dyson prediction, while for $E > E_T$, $\langle n^2(E)\rangle \sim \langle n(E)\rangle^{d/2}$. This is probed in Fig. 1, where the variances $\langle\delta^2 n(E)\rangle$ as a function of $\langle n(E)\rangle$ for 3D, 4D, and 5D samples of different sizes are plotted. In all cases the GOE logarithmic behavior is followed for small energy windows. For energy windows larger than the Thouless energy, $\langle n\rangle > \langle n(E_T)\rangle$, stronger than linear growth sets in. The Thouless energy depends on disorder and dimensionality, and we chose the strength of disorder for each case ($W = 5$ for 3D and 4D samples, $W = 10$ for 5D samples), so E_T will be such that $\langle n(E_T)\rangle$ will be of order O(10–100). Since the dimensionless conductance is defined as the ratio between the Thouless energy and the mean level spacing, $g = E_T/\Delta$, and $\langle n(E_T)\rangle = g$. Above $\langle n(E_T)\rangle$ the variance crosses over to a different behavior and shows a stronger than linear increase. Fitting the variance to an $\langle n(E)\rangle^{\beta}$ behavior shows that beyond the crossover region, there is a wide range for which the power law β is constant, and at even higher energies deviations appear.

This general behavior is seen for all dimensionalities and system sizes. For the 3D case with $W = 5$, the Thouless energy, i.e., where the variance starts to diverges from the Wigner-Dyson (GOE) predictions, appears around $\langle n(E_T)\rangle \sim 20$. Fitting β after the variance substantially diverges from the logarithmic behavior; that is, the region $50 < \langle n(E)\rangle < 150$ results in $\beta = 1.23, 1.26, 1.31$ for $L = 20, 24, 28$, which seems to hold well up to $\langle n(E)\rangle < 350, 400, 450$, respectively. Above these values, the numerical computed variance tapers off to a more moderate increase. The reason may be finite-size effects or a problem with local unfolding on larger energy scales. For three dimensions we expect $\beta = 1.5$, while the values we see are lower but increase with the system size L. Thus, it may be that for much larger system sizes the predicted value would be reached; nevertheless, extrapolating from the change in β as L increases, we conclude that much larger systems will be needed in order to reach $\beta = 1.5$.

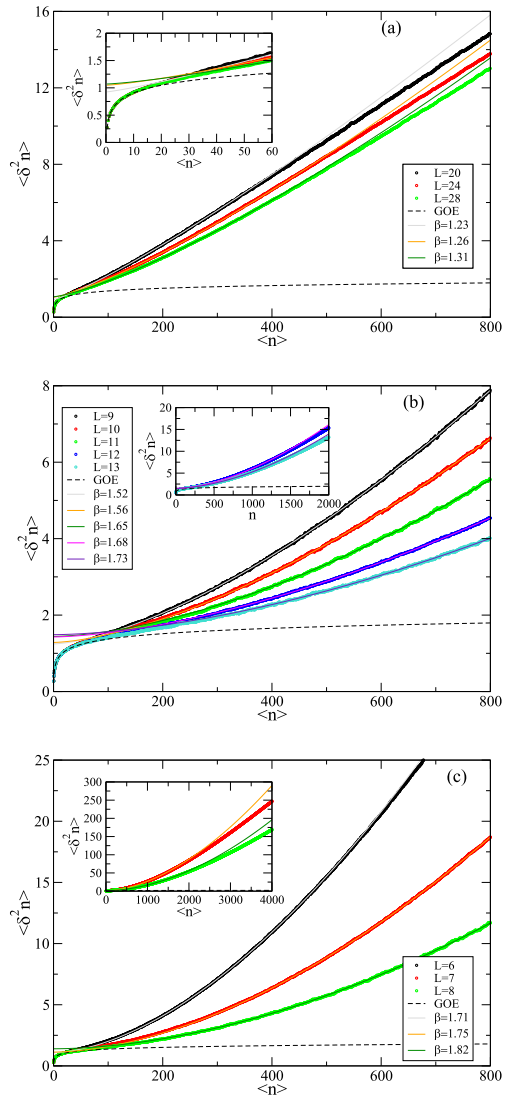

FIG. 1. The variance $\langle \delta^2 n(E) \rangle$ as a function of $\langle n(E) \rangle$ for (a) 3D, (b) 4D, and (c) 5D samples of different sizes. (a) Three-dimensional samples of sizes $L = 20, 24, 28$ and disorder $W = 5$. For $\langle n \rangle < \langle n(E_T) \rangle \sim 20$, Wigner-Dyson (GOE) behavior is followed, as can be seen clearly in the inset. In the region $50 < \langle n(E) \rangle < 150$ a fit to $\langle n(E) \rangle \sim \langle n(E) \rangle^{\beta}$ is performed, resulting in $\beta = 1.23, 1.26, 1.31$ for $L = 20, 24, 28$, respectively. Above $\langle n(E) \rangle > 80$, deviations from the power law become apparent, and the variance increases more moderately. In the inset the deviation from the GOE logarithmic behavior at $\langle n(E_T) \rangle \sim 20$ can be clearly seen. (b) Four-dimensional samples of sizes $L = 9, 10, 11, 12, 13$ and disorder $W = 5$. For $\langle n \rangle < \langle n(E_T) \rangle \sim 80$ Wigner-Dyson (GOE) behavior is followed. In the region $400 < \langle n(E) \rangle < 800$ a fit to $\langle n(E) \rangle \sim \langle n(E) \rangle^{\beta}$ is performed, resulting in $\beta = 1.52, 1.56, 1.65, 1.68, 1.73$ for $L = 9, 10, 11, 12, 13$, respectively. In the inset the behavior for larger values of the energy window is depicted. Clearly, the variance does not continue to grow at the same pace. (c) Five-dimensional samples of sizes $L = 7, 8$ and disorder $W = 10$. For $\langle n \rangle < \langle n(E_T) \rangle \sim 60$, Wigner-Dyson (GOE) behavior is followed, as can be seen clearly in the inset. In the region $200 < \langle n(E) \rangle < 400$ for $L = 6$ and the region $400 < \langle n(E) \rangle < 800$ for $L = 7, 8$ a fit to $\langle n(E) \rangle \sim \langle n(E) \rangle^{\beta}$ is performed, resulting in $\beta = 1.75, 1.83$ for $L = 7, 8$, respectively. Again, as shown in the inset, for larger values of $\langle n(E) \rangle$ a weaker growth in variance appears.

A similar behavior is seen for higher dimensionality. For the 4D case with the same disorder $W = 5$ the Thouless energy is larger, and $\langle n(E_T) \rangle \sim 80$. This is expected because as the number of nearest neighbors to which the particle can hop increases, the effect of disorder should decrease. Again, we fit β for the region for which the variance begins to significantly diverge from GOE, $400 < \langle n(E) \rangle < 800$, $\langle n(E) \rangle \sim \langle n(E) \rangle^{\beta}$, and obtain $\beta = 1.52, 1.56, 1.65, 1.68, 1.73$ for $L = 9, 10, 11, 12, 13$. Once more, values are below the expected power law $\beta = 2$ but get closer as the system size is increased. The same pattern emerges also for 5D samples where the disorder was increased to $W = 10$ so that the Thouless energy would be similar to the value obtained for lower dimensions $\langle n(E_T) \rangle \sim 60$. A fit for the region $400 < \langle n(E) \rangle < 800$ yields $\beta = 1.75, 1.83$ for $L = 7, 8$, far from the expected $\beta = 2.5$. Once more, for 4D and 5D samples, for large energy scales, $\langle n(E) \rangle > 1500$, the increase in the variance tapers.

Thus, although with much effort probing even larger sizes may be possible, it nevertheless does not seem very promising, and we shall turn in a different direction. This direction is based on the singular value decomposition method and is described in the following section.

IV. SINGULAR VALUE DECOMPOSITION

A. General

SVD is a mathematical method applied mainly in the field of data analysis and has enjoyed growing popularity [24]. In this method a matrix X of size $M \times P$ (not necessarily Hermitian or square) is decomposed to a multiplication of three matrices. In general the relevant data are arranged by rows and columns, where the specifics depend on the application. Thus, X is decomposed to $X = U \Sigma V^T$, where U and V are $M \times M$ and $P \times P$ matrices, while Σ is an $M \times P$ *diagonal* matrix of rank, which $r = \min(M, P)$. σ_k stands for the r diagonal elements of Σ are called the singular values (SVs) of X. The SVs are always positive and can be arranged by size so $\sigma_1 \geqslant \sigma_2 \geqslant \cdots \geqslant \sigma_r$. The Hilbert-Schmidt norm of the matrix $||X||_{HS} = \sqrt{\mathrm{Tr} X^{\dagger} X} = \sqrt{\sum_k \lambda_k}$ (where $\lambda_k = \sigma_k^2$). Thus, X can be written as a sum of matrices $X^{(k)}$, where $X_{ij} = \sum_k \sigma_k X_{ij}^{(k)}$ and $X_{ij}^{(k)} = U_{ik} V_{kj}^T$. Since the SVs are ordered by amplitude, the main contribution to X comes from the first m modes, and X may be approximated by $\tilde{X} = \sum_{k=1}^{m} \sigma_k X^{(k)}$, for which $||X||_{HS} - ||\tilde{X}||_{HS}$ is minimal. Thus, if λ_k becomes relatively small for some value m, $\tilde{X}$ could be used as an approximation of X [25,26]. Moreover, by plotting λ_k as a function of its ranking k (known as a scree plot in the context of statistical factor analysis [27]) one may gain some insight into the statistical properties of the data in X.

Here we study an ensemble of M realizations of disorder each with P eigenvalues. For the SVD analysis we construct a matrix X of size $M \times P$ where X_{mp} is the p level of the mth realization. After carrying out SVD on X, the singular value square λ_k are ranked from the largest to the smallest. This approach was applied to the spectrum of disordered systems in several studies [19–22]. As is usual in the SVD analysis in these studies, the first few λ_k $[k \leqslant O(1)]$ correspond to global features of the spectra. Larger SV (λ_k) show a power

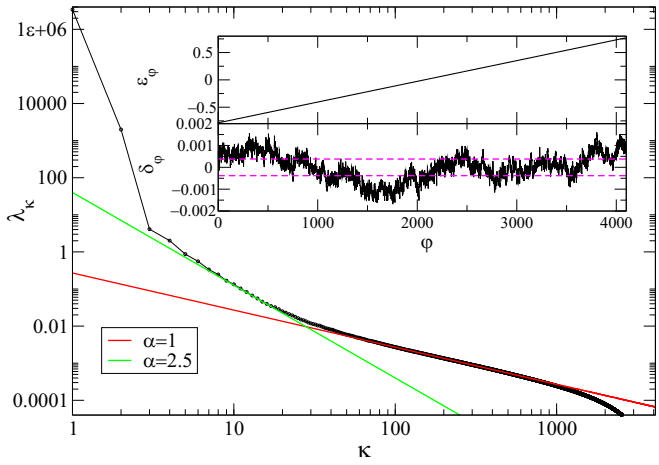

FIG. 2. A scree plot of the ranked singular values for $M = 4096$ different realization of the 3D case of size $L = 28$, where $P = 4096$ eigenvalues around the center of the band are considered. The first two modes $k = 1, 2$ are clearly orders of magnitude larger than the rest. Lower modes seem to follow the power law $\lambda_k \sim k^{\alpha}$. For $3 < k < 20$, $\alpha = 2.5$ fits well, while for $k > 50$, $\alpha = 1$. Inset: The contribution of the first couple of modes to the jth eigenvalue of a particular realization $e_j^{i=1}$ and the contribution of the remaining modes $\delta_j^{i=1}$. The dashed magenta lines indicate a range of $\pm\Delta$ around zero.

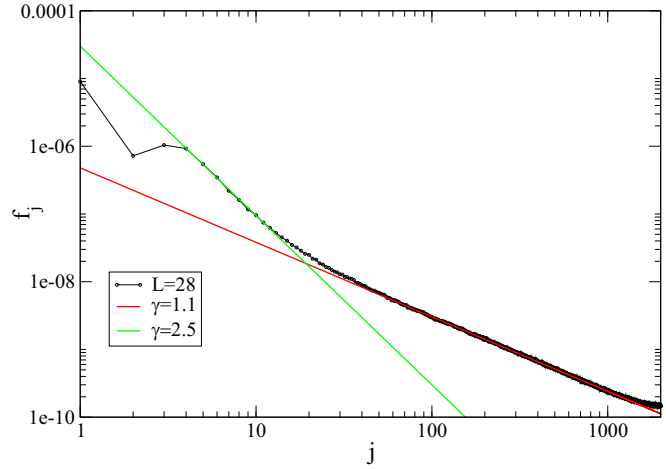

FIG. 3. The power spectrum F_k for the ensemble studied in Fig. 2. Low frequencies ($4 < k < 15$, corresponding to large energy scales) follow the power law $F_k \sim k^{\gamma}$, with $\gamma = 2.5$, while high frequencies ($k > 50$, corresponding to small energies) have $\gamma = 1.1$, within the expected slope for Wigner-Dyson statistics.

law behavior $k^{-\alpha}$ with $\alpha = 2$ at the Poisson regime and $\alpha = 1$ for the Wigner regime.

Here we will examine whether the large-scale behavior of the energy can be gleaned with the help of SVD. We will use two different approaches which will eventually lead to similar results. In the first, we shall use SVD to perform a global unfolding. The second will use the scree plot to tease out the power law behavior of the relevant energy scale.

B. Global unfolding

The idea behind global unfolding using SVD is to filter out the low modes which represent the global behavior while retaining the lower modes that encode local fluctuations. We shall illustrate the global unfolding procedure for an ensemble of realizations for the 3D case of size $L = 28$. As previously described, we construct a matrix X, where each row contains $P = 4096$ eigenvalues around the center of the band for each realization and $M = 4096$ columns representing the different realizations. Matrices U, V, and Σ are numerically extracted, and the $r = M$ diagonal terms σ_k are ranked according to amplitude, from the largest to the smallest. The matrices $X^{(k)}$ are constructed out of U and V, paying attention to the correct sign [28]. As can be seen in Fig. 2 where the SVD values of $\lambda_k = \sigma_k^2$ are plotted, the first couple of modes $\lambda_{k=1,2}$ are clearly orders of magnitude larger than the lower modes. This is a feature common to all the cases considered here. Thus, we may attribute the global features of the spectrum to the first two modes and the local fluctuations to the rest.

We define the contribution of the first couple of modes to the jth eigenvalue of the ith realization as $e_j^i = \sum_{k=1}^{2} \sigma_k X_{i,j}^{(k)}$, and the contribution of the rest of the modes is $\delta_j^i = \sum_{k=3}^{r} \sigma_k X_{i,j}^{(k)}$. An illustration of the behavior of $e_j^{i=1}$ and $\delta_j^{i=1}$ for the first realization in the ensemble is presented in the inset of Fig. 2. It is obvious that $e_j^{i=1}$ corresponds to the linear increase of the eigenvalues as a function of j expected in the Anderson model around the center of the band (at zero energy). Thus, the broad features of the spectra are captured by these two modes. The local fluctuations are captured by $\delta_j^{i=1}$, and one can see the fast short-range fluctuations and also some longer-range ones. Estimating the mean level spacing Δ from $e_j^{i=1}$ and comparing it to $\delta_j^{i=1}$ (see lower inset in Fig. 2) further strengthens the case for longer-range fluctuations.

This behavior leaves a very clear mark on the scree plot. Fitting the lower modes to a power law $\lambda_k \sim k^{\alpha}$ results in two distinct regions. For $3 < k < 20$, a power of $\alpha = 2.5$ fits well, while $50 < k < 1000$ suggests $\alpha = 1$. Intuitively, one would guess that modes $3 < k < 20$ correspond to longer energy scales for which $E > E_T$ while $k < 50$ correspond to shorter energy scales. Nevertheless, one would like to confirm this assertion.

There has been much work devoted to studying the expression of the statistics of local fluctuations on the power spectrum of these fluctuations. It was shown that the power spectrum of the local fluctuation of chaotic systems is different than the power spectrum of integrable systems [18,29–32]. Specifically, the power spectrum of the local fluctuations for each realization is defined as

$$F_k^i = \left| \frac{1}{r} \sum_{j=1}^{r} \delta_j^i \exp\left(\frac{-2\pi i k j}{r} \right) \right|^2, \tag{2}$$

and averaging over all realizations $F_k = \langle F_k^i \rangle$. For chaotic systems $F_k \sim k^{-1}$, while for integrable (localized) systems $F_k \sim k^{-2}$. The power spectrum of the local fluctuations for the 3D case of size $L = 28$ is presented in Fig. 3. As for the singular value modes, two regimes are apparent. The high frequencies follow the power law $F_k \sim k^{-\gamma}$, with $\gamma = 1.1$, while after a crossover a range of low frequencies fits to $\gamma = 2.5$. Thus, for the high frequencies ($k > 50$, corresponding to

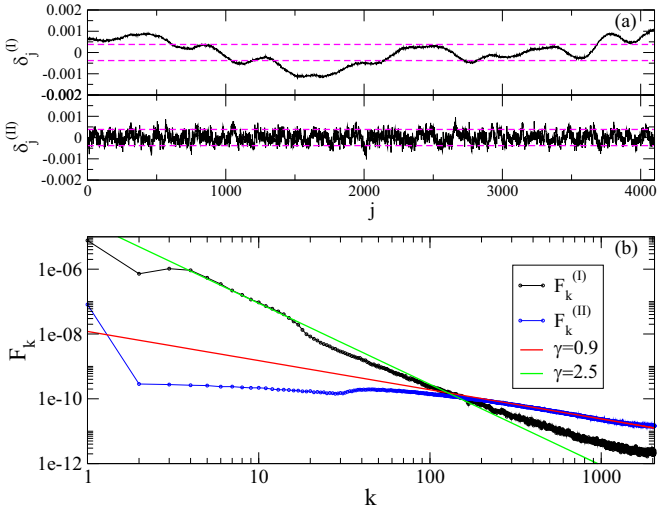

FIG. 4. (a) The contribution of the lower modes ($3 < k < 30$) $\delta_j^{i=1(\mathrm{I})}$ and the higher modes ($31 < k < r$) $\delta_j^{i=1(\mathrm{II})}$ to the jth eigenvalue of a particular realization $i = 1$. The dashed magenta lines indicate $\pm\Delta$ (average level spacing). A clear difference between the low modes which encode long-range fluctuations and the higher modes which represent short-range fluctuations is apparent. (b) The power spectrum $F_k^{(\mathrm{I,II})}$ of $\delta_j^{i(\mathrm{I,II})}$. The low modes' power spectrum $F_k^{(\mathrm{I})}$ shows a slope of $\gamma = 2.5$ for the low frequencies ($4 < k < 20$) and tapers for higher frequencies. The power spectrum $F_k^{(\mathrm{II})}$ for the higher modes reveals that these modes correspond to high frequencies at the range $k > 100$, with slope $\gamma = 0.9$.

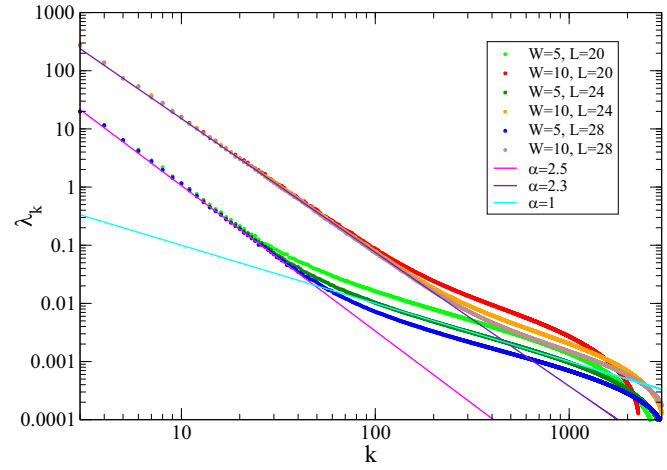

FIG. 5. The SVD mode scree plot for 3D systems where an ensemble of $M = 3000$ realizations of disorder and sizes $L = 20, 24, 28$ are considered. In all cases $P = L^3/2$ eigenvalues around the center of the band are taken into account. Two different strengths of disorder, $W = 5$ and $W = 10$, for all sizes are presented. Lines depict different slopes $\lambda_k = k^{-\alpha}$, with $\alpha = 2.5, 2.3, 1$.

small energies), the behavior of the power spectrum is close to what was observed in other chaotic (GOE) systems [18,29–32]. There are a couple of interesting observations that one can draw from the behavior of the low frequencies. The first has to do with the equivalence between the power laws of the SVD scree plot for low modes and the power law at low frequencies, i.e., $\alpha = \gamma = 2.5$, and for the high modes and frequencies $\alpha \sim \gamma \sim 1$. Such correspondence between the power law of the SVD modes and power spectrum frequencies was noted for the energy spectrum in Refs. [19–22] and elucidated in Ref. [33]. The correspondence also determines the energy scale of the singular values. The kth Fourier transform frequency corresponds to an energy scale $P\Delta/2k$; thus, the region for which GOE statistics holds is of the order of 40Δ, not too far from the estimation of the Thouless energy obtained via the number variance. As can be seen in Fig. 2, also the singular value modes follow the GOE expectation ($\alpha = 1$) up to $k = 50$. Moreover, both curves show a similar behavior, and one may assume that the scree plot depicts the same physics as the power spectrum of the globally unfolded energy spectrum and that the energy scales probed by the modes of the SVD are similar to the energy scales of the Fourier transform.

In order to substantiate the proposed connection between the energy scale and the SVD mode number, we split the contribution of the modes into two parts: $\delta_j^{i(\mathrm{I})} = \sum_{k=3}^{30} \sigma_k X_{i,j}^{(k)}$ and $\delta_j^{i(\mathrm{II})} = \sum_{k=31}^{r} \sigma_k X_{i,j}^{(k)}$. As can be seen in Fig. 4(a) for the same realization presented in the inset of Fig. 2, $\delta_j^{i(\mathrm{I})}$ indeed depicts longer-range fluctuations, while $\delta_j^{i(\mathrm{II})}$ portrays short-scale fluctuations. This can be confirmed by the power spectrum of the fluctuations $\delta_j^{i(\mathrm{I,II})}$. For the low singular value modes the corresponding power spectrum [see Fig. 4(b)] frequencies are in the range of $4 < k < 20$ with the same power law $\alpha = \gamma = 2.5$, while for the higher modes the corresponding frequencies are at $k > 100$ with a slope $\gamma = 0.9$. Thus, one can reasonably conclude that low modes in the SVD probe the large energy scales of the spectrum.

Another observation is that both for the power spectrum and for the SVD scree plot the lower frequencies and modes exhibit a power law with a slope of $1 + d/2$. The slope of the power spectrum could be generally associated with the value of the power of the variance [34,35]. As detailed in the Appendix, indeed, the expected value of the power spectrum $\gamma = 1 + d/2$ can be analytically explained. In the next section we will further substantiate these observations.

C. Scree plot

As we have previously seen, the scree plot of the singular values characterizes the behavior of the large energy scale by showing a power law behavior of the low modes corresponding to $1 + d/2$ power, clearly distinct from $\alpha = 1$ seen for higher modes. Here we check whether this behavior is robust for different system sizes, disorder strengths, ranges of the spectrum, and dimensionalities.

First, we continue to present results for the SVD mode scree plot for 3D samples in Fig. 5. All results are for an ensemble of $M = 3000$ different realizations at each size and disorder strength. Three different sizes, $L = 20, 24, 28$, are considered, each for two different strengths of disorder, $W = 5$ [which, as we saw, corresponds to $n(E_T) = g = 20$] and $W = 10$ [$n(E_T) = g = 5$, which makes sense since $E_T \sim 1/W^2$]. Thus, for the $W = 5$ samples we are deep in the metallic regime where Altshuler and Shklovskii's predictions are expected to hold, while for $W = 10$ we are already closer to the localized regime ($g = 1$). Indeed, we can see that the

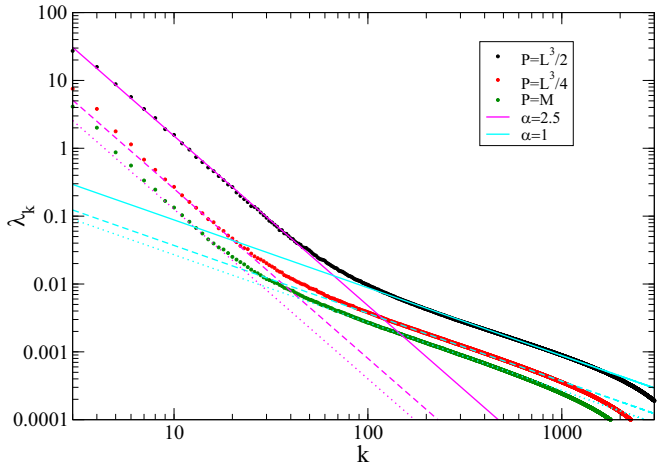

FIG. 6. The SVD mode scree plot for 3D systems ($M = 4096$ realizations) of size $L = 28$. Three different ranges of eigenvalues straddling the center of the band are presented: $P = L^3/2 = 10\,976$, $P = L^3/4 = 5488$, and $P = M$. The qualitative behavior of the slopes, i.e., $\alpha = 2.5$ (magenta line) for low modes and $\alpha = 1$ for higher modes (cyan line), does not change, although the crossover occurs at smaller values of k as P becomes smaller.

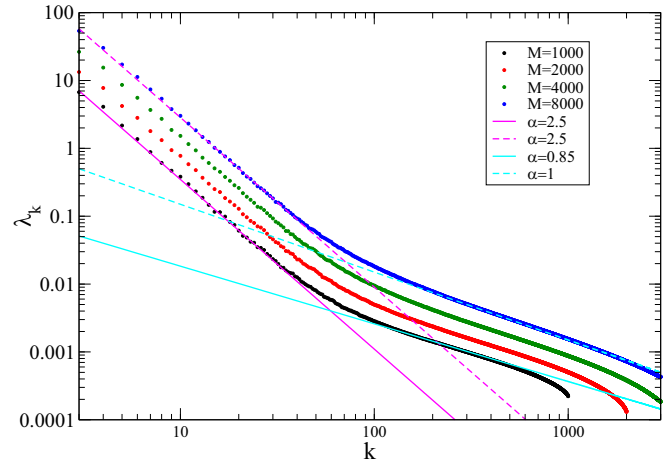

FIG. 7. The SVD mode scree plot for 3D systems of size $L = 28$ and different numbers of realizations $M = 1000, 2000, 4000, 8000$ for the same $P = L^3/2 = 10\,976$. The behavior of the low mode slopes is not sensitive to the ensemble size, and a slope of $\alpha = 2.5$ is seen for all values of M. Lower modes are more susceptible to the number of realizations. For small values of $M = 1000$ the slope fits $\alpha = 0.85$ for $M = 1000$ at higher modes, while it shifts to $\alpha = 1$ at $M = 8000$.

range of modes for which the GOE behavior holds ($\alpha \sim 1$) is much lager for the weaker disorder. The weak disorder singular values fall on top of each other for the lower modes, with a slope of $\alpha = 2.5 = 1 + d/2$. Then for higher modes the slope switches to the GOE behavior ($\alpha \sim 1$) where the value of k for which the switch occurs is higher as the system size increases. We speculate that this is the result of the fact that for larger systems there are more eigenvalues in the range of $L^3/2$. We shall further substantiate this assertion shortly. A similar behavior is seen for the stronger disorder ($W = 10$), although the slope deviates a bit from $\alpha = 1 + d/2$ and is closer to $\alpha = 2.3$. This is not surprising since the predictions in Ref. [7] were obtained using diagrammatic reasoning, strictly valid only deep in the metallic regime ($g \gg 1$).

In Fig. 6 we examine the influence of the change in the range of the eigenvalues P on λ_k. Indeed, the main influence of narrowing the range of P is to shift the crossover from the $\alpha = 2.5$ slope to the GOE $\alpha = 1$ slope to lower values of k. This makes sense since the smaller the range is, the smaller the number of energies larger than the Thouless energy is in this range. Thus, when one wants to focus on energies beyond the Thouless energies and there is a limit on the ensemble size M, one should expand P to the largest available range, even if $P \gg M$.

The number of realizations taken in the ensemble M also plays a role in the behavior of the SVD modes. As can be seen in Fig. 7, the slope for the low mode does not depend on the number of realizations in the ensemble M and remains $\alpha = 2.5$ for all values of M. On the other hand, for the high modes the slope varies from $\alpha = 0.85$ at $M = 1000$ to $\alpha = 1$ for the largest number of realizations $M = 8000$, in line with the predictions for the Wigner-Dyson statistics. Such behavior was previously seen in the study of the generalized Rosenzweig-Porter model where the scree plot of the SVD modes for large k (the GOE regime) also follows a slope of $\alpha \sim 0.8$ [22] for small values of M. This behavior was attributed there to the fact that $M \ll P$. This fits well with our current results where, as M grows, α is closer to 1.

Finally, we wish to examine the dependence on dimensionality of the SVD modes. As we have seen for $d = 3$ and argued analytically, we expect to observe a slope of $\alpha = 1 + d/2$ for the lower modes crossing over to a slope of $\alpha = 1$ at higher modes. Indeed, the scree plot shown in Fig. 8 confirms that the slope of the low modes corresponds to $\alpha = 3$, and $\alpha = 3.5$ for $d = 4$ and $d = 5$, as expected from the number variance behavior at large energies predicted in Ref. [7]. Higher modes show a slope of $\alpha = 0.95$ for both $d = 4$ and $d = 5$, close to the expected value of $\alpha = 1$, except for the largest length at each dimensionality for which the number of realizations $M = 1000$ is smaller than for the other length, and the slope is $\alpha = 0.83$. This is in line with the behavior shown in Fig. 7.

V. DISCUSSION

The detection of the Thouless energy in the spectrum of weakly disordered chaotic systems has long been achieved by detecting the deviation from the expected Wigner Dyson logarithmic dependence of the number variance. Thus, it could be assumed that the number variance will also reveal the behavior of the spectrum at energy scales beyond the Thouless energy derived by Altshuler and Shklovskii [7]. Indeed, a stronger than linear dependence has frequently been observed; nevertheless, extracting the expected power law behavior from the number variance after local unfolding has turned out to be far from trivial. As has been shown here, the number variance does, indeed, show an $\langle n^2(E)\rangle \sim \langle n(E)\rangle^\beta$ behavior for a significant range of levels. Although the value of β rises as the size of sample increases towards the expected $d/2$ value, it remains hard to extrapolate a value with the largest samples we are able to compute.

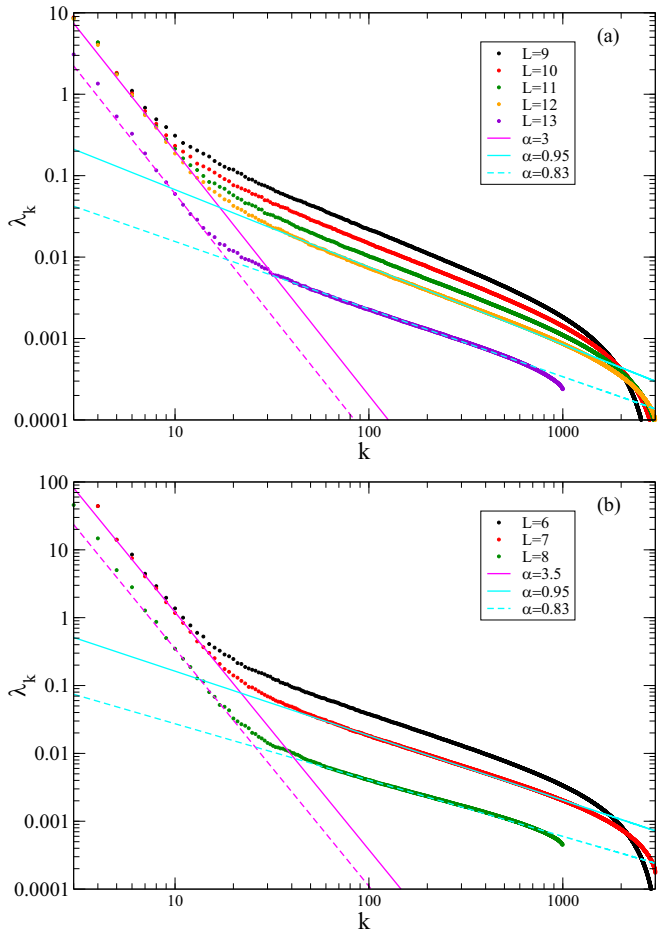

FIG. 8. The SVD mode scree plot for (a) 4D and (b) 5D systems ($M = 3000$ realizations, except for the largest size in each case where $M = 1000$) of sizes $L = 9, 10, 11, 12, 13$ for the 4D case and $L = 6, 7, 8$ for 5D realizations of disorder $W = 5$ (4D) and $W = 10$ (5D). The number of eigenvalues $P = L^3/2$. For both dimensionalities the low mode slopes follow a $1 + d/2$ behavior, i.e., $\alpha = 3$ for $d = 4$ and $\alpha = 3.5$ for $d = 5$, and a slope close to 1 ($\alpha = 0.95$) for the higher modes except at the largest sizes where $\alpha = 0.83$.

By taking the route of the SVD, it is possible to overcome these difficulties. The SVD essentially decomposes the spectrum to modes where the low modes (large amplitudes) capture the longer-range features. As we have shown, the SV modes are, in a sense, similar to the Fourier transform frequencies and show similar regularities of the frequencies and modes. Nevertheless, the SVD saves the need to first unfold and then perform a power analysis over all realizations and finally average; thus, it is a much more concise method. Moreover, since the contribution of the lowest modes e^i_j filtered out is custom set for each realization i, one overcomes the problem of individual realization global variations raised in Ref. [15]. Thus, either by unfolding with SVD and then performing a power spectrum or by directly examining the singular values using the scree plot, it is possible to extract the properties of the energy spectra beyond the Thouless energy and to see the predictions of Ref. [7] clearly hold.

This success might encourage the application of the SVD method to other systems for which interesting long-range properties of the energy spectrum are expected such as the SYK model and systems which show many-body localization.

APPENDIX: CONNECTION BETWEEN THE NUMBER VARIANCE AND THE POWER SPECTRUM

Here we aim to show that the relation between the slope of the power spectrum $\langle F_k\rangle \propto k^{-\gamma}$ and the slope of the number variance $\langle \delta^2 n(E)\rangle \propto \langle n(E)\rangle^{d/2}$ is $\gamma = 1 + d/2$.

Following McDowel *et al.* [34], the local fluctuations $\tilde{\delta}^i_j = \delta^i_j/\Delta$ may be rewritten as

$$\tilde{\delta}^i_j = \frac{1}{k_{\max} - k_{\min}} \sum_{k=k_{\min}}^{k_{\max}} \sqrt{2F^i_k}\cos\left(\mathcal{K}j + \phi^i_k\right), \tag{A1}$$

where $k_{\min}$ and $k_{\max}$ are the ranges for which the power spectrum exhibits a particular power law behavior with slope γ, $\mathcal{K} = 2\pi k/r$, and ϕ_i is a phase. The number variance $\delta^2 n^i_j(E)$ for a particular realization i where the energy window E starts at the energy of the averaged jth eigenvalue $j\Delta$ and ends at $(j + l)\Delta$ ($E = l\Delta$) can be written as

$$\tilde{\delta}^2 n^i_j(l\Delta) = \left(\tilde{\delta}^i_{j+l} - \tilde{\delta}^i_j\right)^2. \tag{A2}$$

Substituting $\tilde{\delta}^i_j$ by Eq. (A1) and averaging over the beginning of the energy window j and the phase ϕ_k, one obtains

$$\begin{aligned}\langle \delta^2 n(l\Delta)\rangle = {} & \frac{1}{r-l}\sum_{j=1}^{r-l}\frac{1}{(k_{\max}-k_{\min})^2} \\ & \times \sum_{k=k_{\min}}^{k_{\max}}\sum_{k\prime=k_{\min}}^{k_{\max}}\frac{2F_k}{(2\pi)^2}\int_0^{2\pi} d\phi_k d\phi_{k\prime} \\ & \times [\cos(\mathcal{K}(j+l)+\phi_k) - \cos(\mathcal{K}j+\phi_k)] \\ & \times [\cos(\mathcal{K}(j+l)+\phi_{k\prime}) - \cos(\mathcal{K}j+\phi_{k\prime})],\end{aligned} \tag{A3}$$

resulting in

$$\begin{aligned}\langle \delta^2 n(l\Delta)\rangle = {} & \frac{1}{r-l}\sum_{j=1}^{r-l}\frac{1}{k_{\max}-k_{\min}}\sum_{k=k_{\min}}^{k_{\max}} \\ & \times \frac{2F_k}{2\pi}\int_0^{2\pi} d\phi_k\{\cos^2[\mathcal{K}(j+l)+\phi_k] \\ & + \cos^2(\mathcal{K}j+\phi_k) - 2\cos[\mathcal{K}(j+l)+\phi_k] \\ & \times \cos(\mathcal{K}j+\phi_k)\}.\end{aligned} \tag{A4}$$

Performing the integration over ϕ_k and summation over j and retaining only the l-dependent part, one obtains

$$\langle \delta^2 n(l\Delta)\rangle \sim \frac{1}{k_{\max}-k_{\min}}\sum_{k=k_{\min}}^{k_{\max}} F_k\cos(\mathcal{K}l). \tag{A5}$$

Replacing the summation with an integration and using the power law dependence of the power spectrum lead to

$$\langle \delta^2 n(l\Delta)\rangle \sim \int_{\mathcal{K}_{\min}}^{\mathcal{K}_{\max}} d\mathcal{K}\mathcal{K}^{-\gamma}\cos(\mathcal{K}l) \sim l^{\gamma-1}. \tag{A6}$$

Thus, since, following Altshuler and Shklovskii [7], $\langle \delta^2 n(l\Delta)\rangle \sim l^{d/2}$, we conclude that the power spectrum should exhibit a slope $\gamma = d/2 + 1$.

[1] M. L. Mehta, *Random Matrices*, 2nd ed. (Academic, New York, 1991).

[2] B. I. Shklovskii, B. Shapiro, B. R. Sears, P. Lambrianides, and H. B. Shore, Phys. Rev. B **47**, 11487 (1993).

[3] T. Guhr, A. Muller-Groeling, and H. A. Weidenmuller, Phys. Rep. **299**, 190 (1998).

[4] Y. Alhassid, Rev. Mod. Phys. **72**, 895 (2000).

[5] A. D. Mirlin, Phys. Rep. **326**, 259 (2000).

[6] F. Evers and A. D. Mirlin, Rev. Mod. Phys. **80**, 1355 (2008).

[7] B. Altshuler and B. Shklovskii, Zh. Eksp. Teor. Fiz. **91**, 220 (1986) [Sov. Phys. JETP **64**, 127 (1986)].

[8] D. Braun and G. Montambaux, Phys. Rev. B **52**, 13903 (1995).

[9] E. Cuevas, E. Louis, M. Ortuño, and J. A. Vergés, Phys. Rev. B **56**, 15853 (1997).

[10] A. M. García-García and J. J. M. Verbaarschot, Phys. Rev. D **94**, 126010 (2016).

[11] A. M. García-García, Y. Jia, and J. J. M. Verbaarschot, Phys. Rev. D **97**, 106003 (2018).

[12] C. L. Bertrand and A. M. García-García, Phys. Rev. B **94**, 144201 (2016).

[13] Á. L. Corps, R. A. Molina, and A. Relaño, Phys. Rev. B **102**, 014201 (2020).

[14] Y. Wang, C. Cheng, X.-J. Liu, and D. Yu, Phys. Rev. Lett. **126**, 080602 (2021).

[15] P. Sierant and J. Zakrzewski, Phys. Rev. B **99**, 104205 (2019).

[16] N. Rosenzweig and C. E. Porter, Phys. Rev. **120**, 1698 (1960).

[17] V. E. Kravtsov, I. M. Khaymovich, E. Cuevas, and M. Amini, New J. Phys. **17**, 122002 (2015).

[18] A. Relãno, J. M. G. Gómez, R. A. Molina, J. Retamosa, and E. Faleiro, Phys. Rev. Lett. **89**, 244102 (2002).

[19] R. Fossion, G. Torres Vargas, and J. C. López Vieyra, Phys. Rev. E **88**, 060902(R) (2013).

[20] G. Torres-Vargas, R. Fossion, C. Tapia-Ignacio, and J. C. López-Vieyra, Phys. Rev. E **96**, 012110 (2017).

[21] G. Torres-Vargas, J. A. Méndez-Bermudez, J. C. López-Vieyra, and R. Fossion, Phys. Rev. E **98**, 022110 (2018).

[22] R. Berkovits, Phys. Rev. B **102**, 165140 (2020).

[23] E. Tarquini, G. Biroli, and M. Tarzia, Phys. Rev. B **95**, 094204 (2017).

[24] C. D. Martin and M. A. Porter, Am. Math. Mon. **119**, 838 (2012).

[25] M. L. Fowler, M. Chen, J. A. Johnson, and Z. Zhou, Signal Processing **90**, 2190 (2010).

[26] H. R. Swathi, S. Sohini, Surbhi, and G. Gopichand, IOP Conf. Ser.: Mater. Sci. Eng. **263**, 042082 (2017).

[27] R. B. Cattell, Multivariate Behav. Res. **1**, 245 (1966).

[28] R. Bro, E. Acar, and T. G. Kolda, J. Chemom. **22**, 135 (2008).

[29] E. Faleiro, J. M. G. Gómez, R. A. Molina, L. Mũnoz, A. Relãno, and J. Retamosa, Phys. Rev. Lett. **93**, 244101 (2004).

[30] J. M. G. Gómez, R. A. Molina, A. Relãno, and J. Retamosa, Phys. Rev. E **66**, 036209 (2002).

[31] L. A. Pachon, A. Relãno, B. Peropadre, and A. Aspuru-Guzik, Phys. Rev. E **98**, 042213 (2018).

[32] J. M. G. Gómez, A. Relãno, J. Retamosa, E. Faleiro, L. Salasnich, M. Vranicar, and M. Robnik, Phys. Rev. Lett. **94**, 084101 (2005).

[33] E. Bozzo, R. Carniel, and D. Fasino, Comput. Math. Appl. **60**, 812 (2010).

[34] E. J. McDowell, X. Cui, Z. Yaqoob, and C. Yang, Opt. Express **15**, 3833 (2007).

[35] D. Krapf, E. Marinari, R. Metzler, G. Oshanin, X. Xu, and A. Squarcini, New J. Phys. **20**, 023029 (2018).